Pis'ma v ZhETF, vol. 76, iss. 10, pp. 742 – 745

Polariton dispersion of periodic quantum well structures

A. V. Mintsev[+], *L. V. Butov*[+*], *C. Ell*[□], *S. Mosor*[□], *G. Khitrova*[□], *H. M. Gibbs*[□]

[+] *Institute of Solid State Physics, RAS, 142432 Chernogolovka, Russia*

[*] *Materials Sciences Division, E. O. Lawrence Berkeley National Laboratory, 94720 Berkeley, California*

[□] *Optical Sciences Center, University of Arizona, 85721 Tucson, Arizona*

Submitted 24 October 2002

We studied polariton dispersion relations of a periodic quantum well structure with a period in the vicinity of half the exciton resonance wavelength, i.e. Bragg structure. We classified polariton modes using an approximation of large quantum well number. The polariton effective masses are found to be very small, $10^{-3} - 10^{-4}$ of the free electron mass.

PACS: 71.35.–y, 71.36.+c

Semiconductor structures allow an engineering of the light-matter interaction. The band structure and dispersion relation of the coupled mode of exciton and photon, called polariton, can be controlled by the structure design, opening great opportunities for fundamental studies of exciton and photon physics as well as for device applications. Recently, considerable attention has been devoted to the study of photon-matter interaction in semiconductor microcavities (MC's) [1] and photonic bandgap materials [2], structures characterized by the size of the light wavelength. One of the advantages of polariton dispersion engineering is the possibility to construct a bosonic quasiparticle with extremely small effective mass, m. In particular, due to the small density of states in such a system, a statistically degenerate gas of polaritons might build up already at high temperatures and small densities (the temperature at which quasi-2D gas of noninteracting bosonic quasiparticles becomes statistically degenerate is $T_0 = \pi\hbar^2 n/2mk_B$ [3]).

In this paper we consider the system of polaritons in a periodic quantum well (PQW) structure with a period in the vicinity of half the exciton resonance wavelength, i.e. in a Bragg structure. In PQW structures, due to the total confinement of excitons in QW's the propagation of polaritons through the PQW is only possible because of electromagnetic transfer of excitation through the barrier layers; in that sense they are Wannier-Mott excitons for in-plane motion and Frenkel excitons for motion in the growth direction [4]. Before there were any experiments, several unique properties of polaritons in PQW structures have been predicted [4 – 9]. Ivchenko et al. [8] made two related and significant predictions. First, in an infinite Bragg structure with $d = \lambda/2$ the normal light wave is a standing wave characterized by two wave vectors $Q = \pm\pi/d$ with a field $E(z) \propto \sin(\pi z/d)$ with nodes at every QW positions. This wave does not couple to excitons because the optical transition matrix element $\propto \int dz E(z)\Psi(z)$ is minimum and, therefore, Bragg PQW structures with a large number of QW's emit and absorb resonant light poorly in the normal direction [8]. Second, although it is a poor emitter, a Bragg structure is an excellent reflector: due to constructive interference between the light waves reflected by the various QW's, the reflectivity of the Bragg structure is dramatically enhanced; in fact, in reflectivity or transmission, a set of N QW's with $d = \lambda/2$ is equivalent to a single QW (SQW) with a radiative coupling coefficient N times amplified over the value for a SQW [8].

The theoretical predictions initiated intense experimental studies. A strong amplification of the reflectance in Bragg PQW structures was observed [10]. The enhancement of the signal decay rate in the Bragg structure was observed in degenerate four-wave-mixing experiments in reflection geometry [11]. Recently, almost 100 % reflectivity and the onset of a photonic band gap were observed in a Bragg PQW sample with $N = 100$ QW's [12]. These experiments verified that the constructive interference between the light waves reflected by the various QW's can be treated as a huge ($\propto N$) enhancement of the radiative coupling coefficient [8]. Further resonant excitation studies revealed that not only are the spectra of transmission, reflection, and absorption dominated by radiative coupling effects but also so is that of resonance Rayleigh scattering [13, 14].

In this paper, we study polariton dispersion relations of high quality Bragg and nearly Bragg PQW structures with $d \approx \lambda/2$. In our experiments e-h pairs are generated by continuum absorption and lose energy by incoherent processes, populating low energy carrier and polariton states. As shown in [12], under these conditions

the PL spectra of a PQW structure can not be explained by the radiatively uncoupled incoherent emission of 100 individual QW's but is dominated by cooperative emission from radiatively coupled QW's, i.e. by polaritonic states. Radiative coupling between the QWs is present without any external coherent excitation.

The non-AR coated PQW sample (DBR28) contains $N = 100$ 8.5-nm-thick $In_{0.04}Ga_{0.96}As$ QW's between GaAs barriers (for details see Ref. [12]). The use of low-In-concentration QW's ensures that the background refractive indices of the well and barrier are nearly identical, thereby eliminating the photonic band gap arising from a distributed Bragg-mirror-like reflectivity. The drop off of flux with increased radius during growth on a rotating substrate provides an experimental way to continuously scan d. For cw PL studies, the excitation was provided either by a HeNe laser (excitation energy $\hbar\omega = 1.96$ eV), or by a Ti:Sapphire laser. The excitation was focused to a 50 μm spot. Experiments were performed in a He^4 cryostat at $T = 1.5$ K.

The theoretical analysis of the polariton mode dispersions is based on the transfer matrix approach that describes light propagation through a multiple layered structure by solving Maxwell's wave equation including the corresponding boundary condition at each interface (LDT). According to Refs. [5, 9] the eigenmodes of the selfconsistently coupled light-QW-exciton system in infinite PQW structure obey the dispersion relation

$$\cos(Qd) = \cos(k_z d) - \frac{\Gamma_0 k/k_z}{\omega_0 - \omega - i\Gamma} \sin(k_z d), \qquad (1)$$

where Q is the wave vector of light along the PQW growth direction reduced to the first Brillouin zone, $k = \omega/\hbar c$, $k_z = \sqrt{\varepsilon_b k^2 - k_x^2}$, k_x is the in-plane polariton wave vector, ω_0 is the exciton resonance energy, Γ_0 and Γ are, respectively, the radiative and nonradiative exciton damping constants in a single QW. As it was shown in Ref. [9], for finite QW number N the eigenmodes correspond to the discretized values of the complex wave vector Q. For large N, the values of the wave vector tend to become real and equally spaced and Eq. (1) transforms to

$$\cos(Q_j d) = \cos(k_z d) - \frac{\Gamma_0(\omega_0 - \omega)k/k_z}{(\omega_0 - \omega)^2 + \Gamma^2} \sin(k_z d), \quad (2)$$

where $Q_j = \frac{\pi}{d}\frac{j}{N}, j = 1, ..., N$. The roots of the Eq. (2) $\omega = \omega(j, k_x)$ correspond to the eigenenergies of the polariton modes. The polariton energies also tend to become real for large N and, therefore, since the imaginary part of the energies yield the radiative width of PQW polaritons, polariton states become stationary in the high N limit, similar to bulk polaritons [7, 9].

The origin of the polariton modes in PQW structures can be understood with the schemes shown in Fig.1. Fig.1a shows schematically dispersion of polaritons in

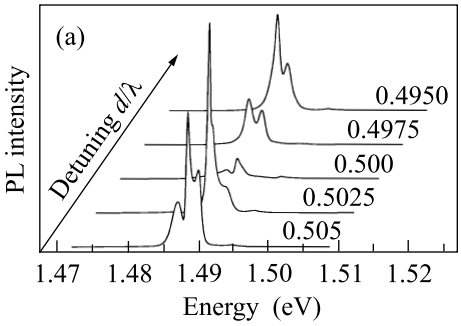

Место для тонового рисунка

Fig.1. (a) The scheme showing the dispersions of polaritons in PQW structures. In infinite periodic structures the polariton dispersions in the PQW growth direction (dotted lines) are constructed from the photon dispersions (bold lines), their replicas (thin lines), and exciton dispersion (dotted line). The polariton branches obey Eq. (2). The transition from infinite to finite number of QW's, N, corresponds to the transition from continuous Q to discrete modes. For large N the energies of the discrete modes (dots) fall on the continuous branch dispersions at $Q_j = \frac{\pi}{d}\frac{j}{N}$, $j = 1, ..., N$ (vertical dashed line). (b) An example of in-plane dispersions of polariton mode branches calculated using Eq. (2). Dotted lines represent dispersions of the exciton and standing waves of light. The polariton mode dispersions (solid lines) are formed by anti-crossing dispersions of the exciton and photon

the PQW growth direction. For infinite N the polariton dispersions are constructed from the photon dispersions, their replicas, and exciton dispersion. We con-

centrate below on the energy region close to the exciton resonance. Around ω_0, there are three PQW polariton branches originating from the folded photon dispersion and exciton dispersion: the upper (U), the middle (M), and the lower (L). The splitting between the branches at the anticrossing point at $Q = \pi/d$, proportional to the electromagnetic coupling between the photon and exciton, is small compared to ω_0 and is exaggerated in Fig.1a. For finite and large N, the energies of the discrete modes fall on the continuous branch dispersions at the momenta $Q_j = \frac{\pi}{d}\frac{j}{N}, j = 1, ..., N$, for the j-th polariton mode, i.e. the continuous branch and discrete modes obey Eq. (2) with the same r.h.s. We mark the upper j-th mode as U_j and so on. Figure 1a presents the case of a Bragg structure with $d = \lambda/2$, i.e. with $\omega_0 = \pi c/d\sqrt{\varepsilon_b}$, the variation of the scheme for different d is straightforward. An example of the in-plane dispersions for U, M, and L polariton branches is shown in Fig.1b. The dispersions were calculated using Eq. (2) for $d/\lambda = 0.501$, $Q_j = 0.99\pi/d$ and $\Gamma_0 = 20\,\mu$eV. The polariton modes are formed by the anti-crossing dispersions of the exciton and standing waves of light (Fig.1b). Note that, the mode M_N is a standing wave with a field $E(z) \propto \sin(\pi z/d)$ with nodes at every QW positions $\forall d$ and $\forall k_x$ and its optical transition matrix element is equal to zero.

Figure 2a shows cw spectra of PL emitted in the direction normal to the PQW structure. Spectra are taken from different positions on the sample corresponding to different period d as labelled in Fig.2a. Figures 2b and 2c present the measured PL energy and intensity of polariton modes at $k_x = 0$ corrected for the exciton energy shift due to the QW thickness change. The radiative mode splitting well exceeds the inhomogeneous exciton linewidth. The solid and dashed lines show positions of the eigenmodes at $k_x = 0$ calculated using Eq. (2). The best agreement between the experiment and Eq. (2) is achieved using $\Gamma_0 = 20\,\mu$eV (dashed lines). The linear fit to reflectivity spectrum HWHM vs N gives a value of $\Gamma_0 = 27\,\mu$eV [12]. The eigenmodes calculated using Eq. (2) with $\Gamma_0 = 27\mu$eV are also shown in Fig.2b. All polariton modes observed in the experiment are clearly classified. This confirms that the QW number $N = 100$ is large enough to validate the approximation of Eq. (2) with real and equally spaced Q_j [9][1)]. Figure 2c shows eigenmodes (solid lines), reflection dips (triangles), and absorption peaks (squares) calculated for

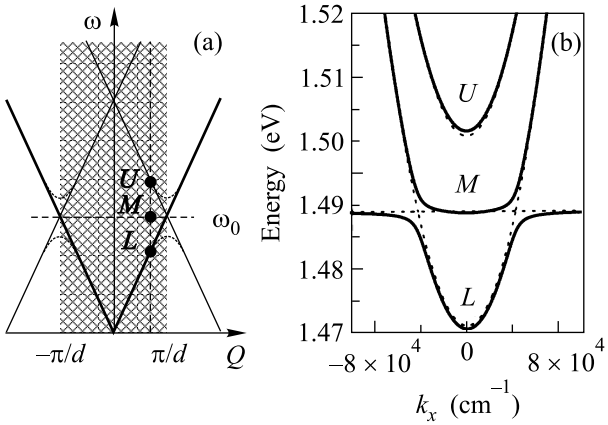

Fig.2. (a) PL spectra in normal direction in reflection geometry for the non-AR coated $N = 100$ $In_{0.04}Ga_{0.96}As/GaAs$ PQW structure under cw nonresonant excitation at 1.96 eV. Spectra are taken from different positions on the sample corresponding to different periods d; $T = 1.5$ K. The poor emission in the normal direction at Bragg resonance, $d = \lambda/2$, reveals the vanishing overlap between the QW excitons and the standing wave of light. (b) The measured PL energy and intensity of polariton modes vs d (greyscale map). The mode energies calculated using Eq. (2) with $\Gamma_0 = 20\,\mu$eV ($\Gamma_0 = 27\,\mu$eV) are shown by dashed (solid) lines. The mode classification includes the branch U, M, or L index and the $j = 1, ..., N$ number, see Fig.1. The optically inactive M_N mode is absent in the PL spectra. (c) Absorption peaks (squares), reflection dips (triangles), and eigenenergies (solid lines) calculated using LDT through a finite non-AR coated 100 QW structure. Note, the functional dependence of A on the period is different for an AR-coated structure

$N = 100$ PQW using a Lorentzian excitonic susceptibility within a LDT approach [12]. Here, the absorption A is defined as $A = 1 - R - T$, where R is the reflection and T is the transmission. The best agreement between the experiment and the theory is achieved using $\Gamma_0 = 27\,\mu$eV in agreement with [12]. As expected, PL clearly follows the absorption, thus the results of the LDT calculations are in good agreement with the experiment.

To measure the dispersion of the PQW polariton modes, we studied angularly resolved PL following experiments in Ref. [15], where this method was applied to study the dispersion of polaritons in MC's. The polariton mode dispersions are revealed via their PL energy vs $k_x = k \sin\phi$ dependence, where ϕ is the external angle between the emitted photon and the direction normal to the PQW structure. The measured dispersions of the polariton modes are presented in Fig.3. The dashed lines show positions of the eigenmodes calculated using

[1)] The calculation of the complex wave vectors Q by using the transfer matrix of the finite 100-QW structure [9] shows that there is a finite imaginary part at periods where the corresponding mode is bright. This implies that the large-N approximation is not validated over the whole range of periods.

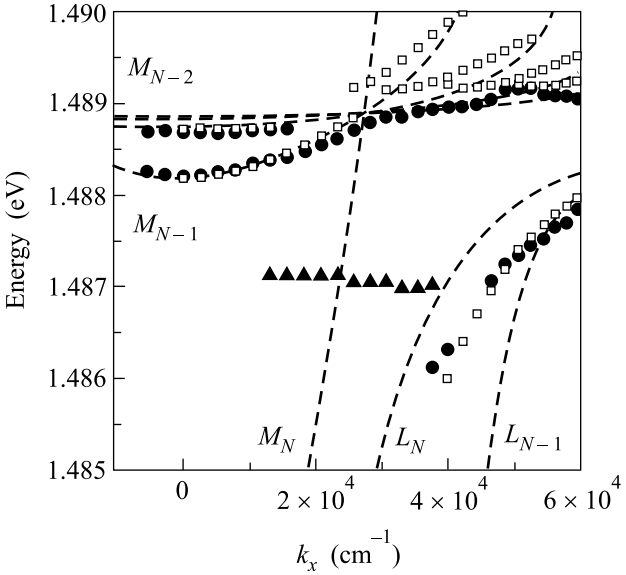

Fig.3. Measured PL energy of polariton modes (solid points) in non-AR coated $N = 100$ $In_{0.04}Ga_{0.96}As/GaAs$ PQW structure with $d = 0.5025\lambda$ vs k_x under cw nonresonant excitation at 1.495 eV; $T = 1.5$ K. Triangles correspond presumably to the PL of localized states. The mode energies calculated using Eq. (2) with $\Gamma_0 = 20\,\mu$eV are shown by dashed lines. The polariton effective masses are extremely small: e.g. the quadratic fit to the mode M_{N-1} dispersion at small k_x yields $m \approx 5 \cdot 10^{-4} m_0$. The calculated absorption peaks using a Lorentzian excitonic susceptibility for the propagation through a 100-QW non-AR coated PQW structure with $\Gamma_0 = 27\mu$eV are shown by open squares

Eq. (2). Dispersions of the polariton modes numerically calculated using LDT for 100 QW's (open squares) are in good agreement with the experimental data, see Fig.3. The calculation based on Eq. (2) has no fitting parameter and uses the value of Γ_0 obtained from the fit to the experimental data in Fig.2. The main result of the polariton dispersion measurement is that the polariton effective masses are very small. In particular, for the mode M_{N-1}, $m \approx 5 \cdot 10^{-4} m_0$, close to the effective mass of microcavity polaritons. This agreement is natural as the polariton dispersions are determined by the anticrossing dispersions of an exciton and standing waves of light both for PQW's and MC's. Note that small density-of-states-effective-mass $[1/m = 2/\hbar^2 \partial E/\partial(k^2)]$ is characteristic for most of the polariton modes (Fig.3).

We notice that the linewidth of the polariton PL from the $N = 100$ PQW sample is sometimes narrower than the linewidth of exciton PL from SQW's grown under as nearly as possible identical conditions. The smallest PL linewidth, ≈ 0.15 meV, observed in $N = 100$ PQW at $d \approx 0.5025\lambda$ is ≈ 4 times narrower than the exciton PL linewidth in the SQW's. The effect of the line narrowing due to the radiative coupling between the QW's clearly dominates over broadening effects originating from QW thickness inhomogeneities, etc.

This work was supported by Russian Foundation for Basic Research, INTAS YSF # 01/2-50, NSF AMOP, JSOP (AFOSR and ARO) and COEDIP.

1. For a review, see G. Khitrova, H. M. Gibbs, F. Jahnke et al., Rev. Mod. Phys. **71**, 1591 (1999).
2. E. Yablonovitch, Phys. Rev. Lett. **58**, 2059 (1987).
3. A. L. Ivanov, P. B. Littlewood, and H. Haug, Phys. Rev. **B59**, 5032 (1999).
4. L. V. Keldysh, Superlattices Microstruct. **4**, 637 (1988).
5. E. L. Ivchenko, Fiz. Tverd. Tela (St. Petersburg) **33**, 2388 (1991) [Sov. Phys. Solid State **33**, 1344 (1991)]
6. L. C. Andreani, Phys. Lett. **A192**, 99 (1994).
7. D. S. Citrin, Solid State Commun. **89**, 139 (1994).
8. E. L. Ivchenko, A. I. Nesvizhskii, and S. Jorda, Fiz. Tverd. Tela (St. Petersburg) **36**, 2118 (1994) [Phys. Solid State **36**, 1156 (1994)].
9. L. C. Andreani, Phys. Stat. Sol. **(b)188**, 29 (1995).
10. V. P. Kochereshko, G. R. Pozina, E. I. Ivchenko et al., Superlattices Microstruct. **15**, 471 (1994).
11. M. Hübner, J. Kuhl, T. Stroucken et al., Phys. Rev. Lett. **76**, 4199 (1996).
12. M. Hübner, J. P. Prineas, C. Ell et al., Phys. Rev. Lett. **83**, 2841 (1999).
13. J. P. Prineas, J. Shah, B. Grote et al., Phys. Rev. Lett. **85**, 3041 (2000).
14. B. Grote, C. Ell, S. W. Koch et al., Phys. Rev. **B64**, 045330 (2001).
15. R. Houdre, C. Weisbuch, R. P. Stanley et al., Phys. Rev. Lett. **73**, 2043 (1994).